RSC Advances

ROYAL SOCIETY OF CHEMISTRY

www.rsc.org/advances

Journal Name

ARTICLE

Study on mediating crystallization behavior of PBT by intermolecular Hydrogen-bonding

Received 00th January 20xx,
Accepted 00th January 20xx

DOI: 10.1039/x0xx00000x

www.rsc.org/

Zhiyuan. Shen,[ab] Faliang. Luo,[*b] Hongcun. Bai,[*b] Pengfei. Si,[b] Xiaomei. Lei,[b] Shengfang. Ding[b] and Lijie.Ji[a]

The intermolecular hydrogen-bonding could be formed between Poly (butylene terephthalate) (PBT) and 4, 4′-thiodiphenol (TDP) which was verified by advanced quantum-chemistry calculation. The blends of PBT and TDP were prepared by melt blending and the intermolecular hydrogen-bonding is characterized by Fourier transform infrared spectroscopy (FTIR). The results showed that intermolecular hydrogen-bonding formed between the carbonyl group of PBT and hydroxyl group of TDP, the carbonyl and hydroxyl absorption bands shifted to a lower wavenumber and the shape of hydroxyl peaks became wider asymmetrically with the TDP content increasing. The effects of hydrogen bonding on the crystallization and melting behaviors of PBT were investigated by differential scanning calorimetry (DSC), polarized optical microscopy (POM) and wide angle x-ray diffraction (WAXD). The results showed that both the non-isothermal melt-crystallization behavior and isothermal crystallization kinetics of PBT were inhibited by addition of TDP. The overall isothermal crystallization rates of PBT in the PBT/TDP blends were obviously slower than that of pure PBT at the same crystallization temperature. The crystal structure of PBT did not change by the incorporation of TDP, while the crystallinity and the crystal size of PBT decreased with the increasing of TDP content.

1 Introduction

Poly (butylene terephthalate) is one of the most important engineering thermoplastic materials due to its good chemical resistance, thermal stability, excellent processability and has wide application in many fields such as electrical components, automotive, precise instruments and many metal replacements.[1-5] However, the crystallization rate is so fast which results in flexural deformation of final products. Therefore, it is meaningful to overcome the defects of flexural deformation of final products by adjusting the crystallization behaviors. Generally, incorporation other polymers including polycarbonate (PC)[6] and poly(ethylene octane) (POE)[7] into PBT to adjust crystallization rate of PBT have been favored for easily realized. Nevertheless, the poor compatibility of the polymer blends was usually a big problem. Recent years, with fast development of nanotechnology, it has offered the possibility to mediate the crystallization and physical properties of polymers such as PBT. Organo-montmorillonite (OMMT) can increase the degree of crystallinity of PBT reported by Chow.[8] Fang et al reported that the multiwalled carbon nanotubes acted as nucleating agent which greatly increasing the crystallization rate of PBT/multiwalled carbon nanotubes nanocomposites.[9] Bian et al. described that microwave exfoliated graphite oxide nanosheets (MEGONSs) as a hetero-nucleating agent for PBT and MEGONSs facilitated the crystallization of PBT.[10] The mediation of the crystallization of PBT may also be achieved by the blending with some filler. Deshmukh et al.[11, 12] found that interfacial interaction between functional groups of filler and polymer would affect the overall crystallization process of PBT by comparative analysis on the effects of functional fillers including $CaCO_3$, nano$CaCO_3$, wollastonite and talc on the crystallization of PBT and the results revealed that $CaCO_3$, wollastonite and low amount of nano$CaCO_3$ would accelerate the crystallization rate of PBT, but the crystallization of PBT was inhibited because of the formation of chemical bonding interaction between talc and PBT. Furthermore, a novel technique was employed for mediate the crystallization of PBT by blending with a reactive solvent (epoxy) has been carried out and the overall crystallization rate of PBT at all temperatures increased with the incorporation of epoxy resin.[13] In addition, some kind of low molecular weight additive, especially some low molecular weight dihydric phenols may obviously change the crystallization-melt behaviors and mechanical and other properties of the polymers for the formation of intermolecular hydrogen-bonding between phenol group and carbonyl, ether, ester, or other proton-acceptor functional groups of polymers. It was reported that bisphenol A (BPA) inhibited the overall isothermal crystallization kinetics and the spherulite growth rate of poly(butylene succinate).[14] Li et al. found that the crystallization of poly(Ɛ-caprolactone) (PCL) was greatly

[a] School of Chemistry and Chemical Engineering, Ningxia University, Yinchuan 750021, China
[b] Key Laboratory of Energy Resource and Chemical Engineering of Ningxia, Ningxia University, Yinchuan 750021, China. E-mail: flluo@iccas.ac.cn Fax: +86 951 2062323;Tel:+86 951 2062393; hongcunbai@gmail.com Fax: +86 951 2062323;Tel:+86 951 2062008

hindered by the addition of 4, 4'-dihydroxydiphenyl ether (DHDPE), when the content of DHDPE reached 40%, PCL changed to be a fully amorphous elastomer.[15] He et al. found that the thermal and dynamic mechanical properties of poly(L-lactic acid) (PLLA) and the physical properties of Poly (3-hydroxybutyrate) [P (3HB)] and Poly (3-hydroxybutyrate-co-3-hydroxyvalerate) (PHBV) were greatly modified through blending with 4, 4′ -thiodiphenol (TDP) because of the intermolecular hydrogen-bonding.[16, 17] The blends of dihydric phenols and polymers mentioned above were all prepared by solution blending method. However, the shortcoming of solution blending is that the process is more complicated and time-consuming and solvent has certain harm to the environment. The melt blending method is closer to the actual production process. Besides, it is unknown that whether or not the intermolecular hydrogen-bonding between dihydric phenols and polymers blends prepared by melt blending would be damaged. As far as we know, such research has not been reported so far. Therefore, in this work, TDP was used as a low molecular weight organic crystal mediator to blend with PBT, and PBT/TDP blends were prepared through melt blending method. It is expected that the intermolecular hydrogen-bonding would form between PBT and TDP, and it might have obvious influence on the crystallization behavior of PBT. The intermolecular interaction and crystallization behavior of PBT/TDP blends were investigated by Fourier transform infrared spectroscopy (FTIR), quantum-chemical calculation, differential scanning calorimetry (DSC) and polarized optical microscopy (POM). The crystal structure of PBT was identified by wide angle X-ray diffraction (WAXD).

2 Experimental

2.1 Materials and sample preparation

Poly (butylene terephthalate) (PBT) used in this study was DURANEX® 2002 EF2001 purchased from WinTech Polymer Ltd (Japan) with its density of 1.31 g/cm^3. The viscosity average molecular weight is 1.3×10^5 g/mol measured by Ubbelohde viscometer. 4, 4′ -thiodiphenol (TDP) (AR) was purchased from Meryer Chemical Technology Co. Ltd. (shanghai, China). The chain structure of PBT and the molecular structure of TDP are shown in Fig. 1.

PBT/TDP blends were prepared by melt mixing in a co-rotating twin-screw extruder (type TSZ-30 China). The temperature profiles of the barrel were 240-250-250-240°C from the hopper to the die. Before melt mixing, PBT was dried in a vacuum oven at 120°C for 12 h. Binary blends of PBT/TDP with weight ratio of 100/0, 95/5, 90/10, 80/20, 70/30 wt/wt were prepared for non-isothermal thermal properties, XRD and FTIR analysis. And 100/0, 98/2, 96/4, 94/6 wt/wt of PBT/TDP were prepared for isothermal crystallization analysis.

2.2 Characterizations and measurements

Quantum chemical calculations in this work are conducted under the framework of density functional theory (DFT) combined with the self-consistent field molecular orbital (SCF-MO) method. The DFT exchange-correlation functional is

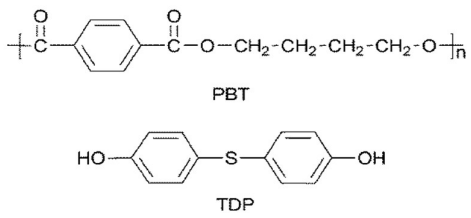

Fig. 1 The chain structure of PBT and the molecular structure of TDP.

treated as Truhlar's M06-2X.[18] We have chosen this specific functional because of the accuracy to explore the system with hydrogen-bonding,[19, 20] which usually plays an important role in the current work. Double-ζ plus double polarization basis sets 6-31G (*d*, *p*) were employed for C, H, O and S. The IR spectroscopic properties were obtained based on the calculations of vibration frequencies on the basis of the optimized geometrical structures at the same theory level. All calculations were performed with the aid of Gaussian09 code throughout the work.[21]

FTIR spectra of PBT/TDP blends were recorded at room temperature by means of a SPECTRUN Two spectrometer (America). The scanned wavenumber range was 4000-400 cm^{-1}. All spectra were recorded at a resolution of 4 cm^{-1} and 32 scans for each sample. Films of the pure PBT and PBT/TDP blends with a thickness suitable for FTIR measurements were prepared in 1 % (wt/wt) chloroform/trichloroacetic acid solution. The ratio of chloroform and trichloroacetic acid in solution was 4:1 (v/v). Then the solution was directly dropped to the surface of KBr plate and dried in a vacuum oven at 100°C for 12 h to remove the solvent. The FTIR measurement of pure TDP was conducted by KBr powder compression method for different sample characteristics and KBr powder was dried in a vacuum oven at 120°C for 12 h before sample preparation.

Differential scanning calorimetry （DSC, TA Q20） was used to study the melting and crystallization behaviors of the blends. The calorimeter was calibrated in temperature and energy using indium. Dry nitrogen was used as purge gas at a rate of 50 ml/min during all the measurements. The samples for all measurements were 4–6 mg.

For recording non-isothermal crystallization process, samples were first heated from 40°C to 260°C at a heating rate of 20°C /min and held at this temperature for 3 min to erase thermal history. Then cooled to 40°C at a heating rate of 10°C /min and subsequently subjected to second melting by heating to 260°C at a heating rate of 10°C /min to determine the melting peak values (T_m).

For the isothermal crystallization process, samples were first heated to 260°C and held for 3 min to erase thermal history, followed by rapid cooling to the selected temperature (T_c) at a cooling rate of 150°C /min. After completing the crystallization, the blends were heated again at 10°C /min until completely melting.

The WAXD measurements were performed at room temperature on a Rigaku D/MARX2200 PC diffractometer using Cu Kα radiation (λ=1.542Å). The measurements were

operated at 40 kV and 30 mA in 2θ ranges from 5° to 40°at a scanning rate of 2°/ min. The samples used for XRD analysis were injection molded using plastic injection molding machine (SZS-15 China).

The spherulite morphologies of pure PBT and PBT/TDP blends were observed by a LEICA DM2500P polarizing optical microscope (Germany). Samples were dissolved in chloroform/trichloroacetic acid solution and then cast on glass substrate. The ratio of chloroform and trichloroacetic acid in solution was 4:1 (v/v). The obtained thin films were melted at 260°C for 3 min to erase thermal history and then rapidly cooled to 202°C at a rate of 70°C /min for isothermal crystallization and kept at this temperature for observations.

The tensile test was carried out at room temperature using a CTM 8050S electrical universal material testing machine (China) at speeds of 10 mm/min. At least five specimens were tested for each recorded value of elongation-at-break.

3 Results and discussion

3.1 Theoretical Investigation of the Hydrogen bond Structure

With the developing of quantum-chemical calculation, it provides more possibility to investigate the intermolecular interaction between PBT and TDP. Fig. 2(a) shows the obtained optimized structures of PBT and (b) scheme of hydrogen-bonding between PBT and TDP, in which OH group of TDP molecule is hydrogen-bonded to C=O group of PBT. The obtained C=O…HO distance (d) is 2.035 Å, which is calculated by:

$$d = \left[(x_i - x_j)^2 + (y_i - y_j)^2 + (z_i - z_j)^2\right]^{1/2} \quad (1)$$

where (x_i, y_i, z_i) and (x_j, y_j, z_j) are atomic Cartesian coordinates of the two atoms. It is noticed that this distance is larger than 0.97 Å for general O–H bonds, while much smaller than 3.75 Å for Van der Waals distance for the interaction of oxygen and hydrogen atoms considering that their Van der Waals radii are 1.55 and 1.20 Å for carbon and hydrogen atoms, respectively.[22] Thus the obtained C=O…HO distance here is within the scope of hydrogen bonding. Table 1 gives the structure parameters obtained from optimized structures (a) and (b) as well as the carbonyl stretching frequencies of pure PBT and hydrogen bonded carbonyl group of PBT. The vibrational frequencies are directly obtained with the aid of Gaussian code by determining the second derivatives of the energy with respect to the Cartesian nuclear coordinates based on:

$$V(R_0 + x) = V(R_0) + \sum_i (\frac{\partial V}{\partial x_i})_0 x_i + \frac{1}{2}\sum_{ij} (\frac{\partial^2 V}{\partial x_i \partial x_j})_0 x_i x_j + \cdots \quad (2)$$

where $x=R–R_0$ is the vector with the displacements of the atomic positions from their equilibria, while the derivatives are calculated at $R=R_0$. In structure (a), the calculated carbonyl stretching frequency of pure PBT is 1864 cm^{-1}, while the carbonyl stretching frequency of hydrogen bonded carbonyl group of PBT is lower by as much as 45 cm^{-1} than pure PBT, meaning that the intermolecular hydrogen-bonding formed between PBT and TDP. Correspondingly, the distance d(C=O (ester)) of pure PBT is 1.204 Å, which is smaller than the d(C=O (ester)) of hydrogen bonded carbonyl group of PBT (1.214 Å). The distance is indeed lengthened, indicating that the hydrogen-bonding also formed between the OH of the TDP and the ester C=O of PBT which cause the lengthening of the carbonyl bond length.

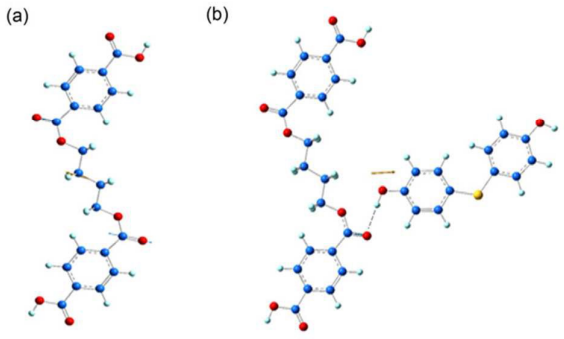

Fig. 2 Optimized structures of (a) pure PBT and (b) hydrogen-bonded PBT and TDP (The blue balls donate the carbon atoms, red balls donate the oxygen atoms and yellow balls donate the sulphur atoms).

Table 1 Calculated C=O stretching frequencies of (a) pure PBT and (b) Hydrogen-Bonded PBT

	υ (C=O) (cm^{-1})	d (C=O) (Å)
(a)	1864	1.204
(b)	1819	1.214

3.2 FTIR analysis on specific interaction between PBT and TDP

In order to make more in-depth studies of the intermolecular hydrogen-bonding of PBT and TDP, experimental technique has been used combined with the theoretical method. FTIR spectroscopy is a particularly suitable technique for investigating a specific intermolecular interaction. The changes of the strength and position of IR absorption peaks resulting from some characteristic functional groups can be attributed to the existence of intramolecular or intermolecular interaction.[15-17, 23, 24] Fig. 3(a) shows the FTIR spectra of the PBT/TDP blends in the carbonyl vibration region. The carbonyl group of pure PBT with its stretching mode locates at 1718 cm^{-1}, whereas TDP shows no absorption in the carbonyl vibration region ranging from 1650cm^{-1} to 1800cm^{-1}. For PBT/TDP blends, the carbonyl absorption band slightly shifted to a lower wavenumber, indicating that the intermolecular hydrogen-bonding formed between carbonyl groups in PBT and the hydroxyl groups in TDP which leading to the variation of carbonyl absorption band. The data shows the high consistency of FTIR experiment and theoretical calculation. In addition, a weak absorption peak is observed in pure PBT at 1681cm^{-1} and it should be ascribed to the intramolecular hydrogen-bonding which usually formed in hydroxyl groups and the carbonyl groups of conjugated system.[25] When adding 5 wt % TDP to PBT matrix, this absorption peak shifted to 1680cm^{-1} and then disappeared gradually with the further increase of TDP content. These observed changes result from switching from the intramolecular hydrogen-bonding of PBT to the intermolecular

hydrogen-bonding between PBT and TDP. The FTIR spectra of PBT/TDP blends in the hydroxyl vibration region are shown in Fig. 3(b). According to Fig. 3(b), Pure TDP has a broad absorption peak in the region from 3000 cm^{-1} to 3650 cm^{-1} and it is attributed to the hydroxyl stretching vibration absorption of hydroxyl group self-association. However, a very weak absorption centered at 3421 cm^{-1} is observed in PBT and it should be attributed to the vibration of hydroxyl groups at the chain terminal of PBT. In PBT/TDP blends, the hydroxyl stretching vibration absorption band shifts to lower wavenumber and the peak shape becomes wider asymmetrically with the TDP content increasing. All these observed variations confirm the formation of hydrogen-bonding between PBT and TDP and this hydrogen-bonding interaction may further influence the crystallization behavior of the PBT in PBT/TDP blends.

3.3 DSC Analysis

According to the analysis above, it is clear that it is not a simple blending of PBT and TDP because of the hydrogen-bonding interaction. Therefore, studying the effect of hydrogen bonding interaction on the melt and crystallization behaviors of the PBT in PBT/TDP blends is essential. The non-isothermal crystallization behavior of pure PBT and PBT/TDP blends is shown in Fig. 4(a). The crystallization exothermal peak (T_c) of pure PBT is sharp and the crystallization peak locates at 193.8°C, indicating the fast crystallization rate of PBT. For PBT/TDP blends, it is obvious that the crystallization exothermal peaks shift dramatically downward to low temperature range and become wider with increasing weight fraction of TDP in the blends. When the TDP content reaches 30 wt%, the value of T_c sharply dropped to 160.8°C, showing a 33.0°C reduction. It was reported that the PC was able to decrease the T_c values of PBT by about 13°C with its content up to 50 wt% and thermotropic liquid crystalline polymer (LCP) decreased the T_c values by 0.6°C with the content of 20wt% at a cooling rate of 10°C/min.[26, 27] The sharply decreased T_c of PBT in the PBT/TDP blends suggests that the formation of hydrogen-bonding interaction between PBT and TDP effectively impedes the movement of molecular chain and suppresses the crystallization ability of PBT. Various thermal parameters determined from the non-isothermal melt and crystallization behaviors are showed in Table 2. It can be seen from Table 2, the crystalline enthalpy (ΔH_c) of pure PBT was measured to be 94.92 $J.g^{-1}$. Moreover, the ΔH_c values were determined to be 80.30, 69.64, 58.99 and 49.03 $J.g^{-1}$ for PBT/TDP blends with the TDP content of 5, 10, 20 and 30 wt%, respectively. The crystallinity of the PBT in the blends was also estimated from the equation 3 and the results are listed in Table 2.

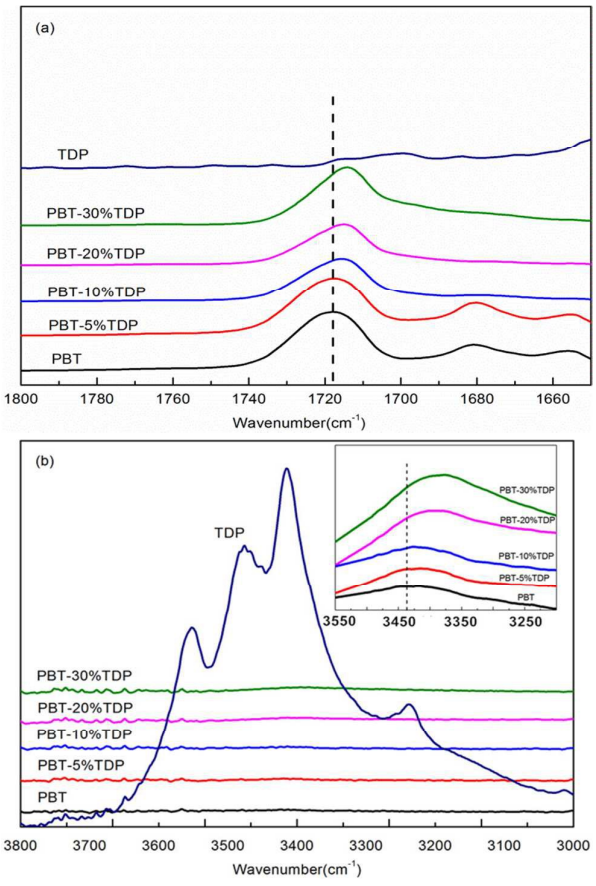

Fig. 3 FTIR spectra in the carbonyl vibration region (a) and hydroxyl vibration region (b) of PBT/TDP blends.

$$X_c = \frac{\Delta H_c}{w_f \Delta H_m^o} \quad (3)$$

where ΔH_c is the measured heat of crystallization for the sample, and ΔH_m^0 is the heat of fusion for a 100% crystalline PBT, which is 142.0 J/g.[28] w_f is the weight percent of the PBT matrix in the blend. From Table 2, the calculations demonstrated that the crystallinity of the PBT in the blends decreases with the increase of TDP content. Fig. 4(b) shows the heating scans of pure PBT and PBT/TDP blends and double melting endotherm peaks of these samples are displayed. The double melting behavior of these samples can be ascribed to melting-recrystallization phenomena during the heating process.[29] The low melting peak (T_{m1}) is associated with the fusion of imperfect crystals grown by normally primary crystallization and the high melting peak (T_{m2}) is for the more perfect crystals formed after recrystallization. Besides, it can be observed that the intensity of T_{m2} decreased with the increasing content of TDP, indicating that the imperfect crystals were relatively prone to be existed and the recrystallization of PBT was less easy to occur because of the hydrogen bonds interaction. Moreover, the decrease of melting temperature and melting enthalpy of the blends with the increasing TDP content reconfirms the conclusion that hydrogen-bonding interaction between the PBT and TDP suppresses the crystallization ability of PBT.

3.4 Isothermal crystallization kinetics

The non-isothermal melt and crystallization behavior of PBT and PBT/TDP blends were investigated in the above section and all of the results showed that the crystallization behavior of PBT was hindered by the intermolecular hydrogen-bonding formed between PBT and TDP. To further confirm the

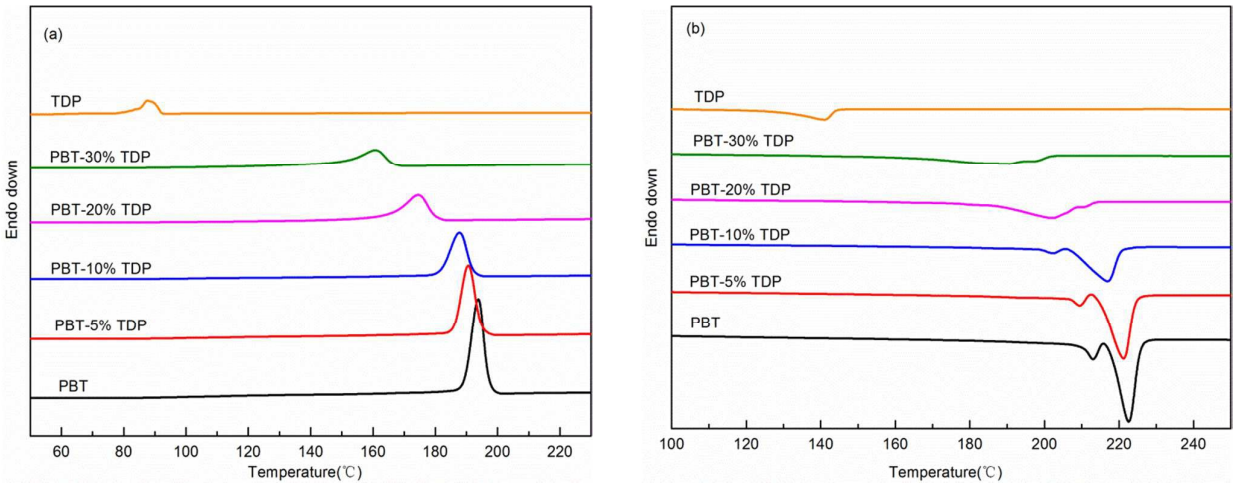

Fig. 4 DSC curves for PBT and PBT/TDP blends (a) cooling curves (10°C /min) and (b) heating curves (10°C /min).

Table 2 Parameters of PBT and PBT/TDP blends obtained from the non-isothermal crystallization at a cooling rate of 10°C /min

PBT/TDP (wt/wt %)	T_c （℃）	$T_{c(onset)}$ （℃）	ΔH_c （J.g^{-1}）	T_{m1} （°C）	ΔH_{m1} （J.g^{-1}）	T_{m2} （°C）	ΔH_{m2} （J.g^{-1}）	X_c (%)
100/0	193.8	197.1	94.92	213.0	12.34	222.6	61.45	66.85
95/5	190.6	194.7	80.30	209.3	9.10	221.2	66.31	59.53
90/10	187.7	192.2	69.64	202.1	4.03	216.8	50.26	54.49
80/20	174.5	180.1	58.99	183.9	-		58.86	51.93
70/30	160.8	166.6	49.03	158.8	-		52.49	49.33

inhibitory effect of TDP on the crystallization rate of PBT, it is necessary to study the isothermal crystallization kinetics of PBT/TDP blend system. However, we are aware that the temperature may be one of the important factors that affect the hydrogen-bonding. The isothermal crystallization temperature of PBT is usually above 200°C. Under such isothermal crystallization temperature, is there the hydrogen-bonding still exist? So molecular dynamics (MD) simulations are conducted by using the atom centered density matrix propagation (ADMP) model[30-32] at M06-2X/6-31G(*d*, *p*) theory level at the 202°C (that is the crystallization experimental temperature in this work) for 2 ps with the time step size as 1 fs. It is found that the hybrid PBT/TDP structure at the end of MD simulation exhibit no much difference compared with that at room temperature. The obtained distance for C=O…HO interaction is also within the scope of hydrogen-bonding (2.198 Å), though it is a bit longer than 2.035 Å at room temperature for temperature rising. Thus it is true that the hydrogen-bonding still form between PBT and TDP under isothermal crystallization temperature. Fig. 5 shows the relation curves between relative crystallinity ($X(t)$) and crystallization time for PBT and PBT/TDP blends at crystallization temperature of 206°C. For the sake of brevity, only the isothermally crystallized at 206°C is listed, while other similar results have also been observed for PBT/TDP blends at crystallization temperatures of 198, 200, 202 and 204°C. The value of $X(t)$ is calculated according to the following equation.

$$X_t = \frac{\int_0^t \frac{dH(t)}{dt} dt}{\int_0^{t\infty} \frac{dH(t)}{dt} dt} = \frac{\Delta H_t}{\Delta H_\infty} \quad (4)$$

where ΔH_t is the total heat evolved at time t and ΔH_∞ is the total heat evolved as time approaches infinity. From Fig. 5, the values of crystallinity up to 100% corresponds to the time is about 12 minutes for PBT, while 62 minutes for PBT/TDP blends with 6 wt% TDP, the total crystallization time is extended about 50 min. The required time is continue increasing for achieving complete crystallization with increasing TDP content at a certain crystallization temperature. It indicates that the formed hydrogen-bonding dramatically suppress the crystallization of PBT.

The Avrami equation is widely used to describe the isothermal crystallization behavior of polymer and polymer blends, as follows:

$$X_{(t)} = 1 - exp(-kt^n) \quad (5)$$

equation (5) can also be converted to:

$$ln\left[-ln\left(1 - X_{(t)}\right)\right] = lnk + nlnt \quad (6)$$

where k is the Avrami rate constant containing the nucleation and the growth parameters, n is the Avrami exponent dependent on the mechanism of nucleation and the form of crystal growth. Figure 6 shows the Avrami plot for pure PBT and PBT/TDP blends isothermally crystallized at 206°C. It can be seen that each curve shows an initial linear portion, but some points

deviate from Avrami equation. The early non-linear stage corresponds to the primary crystallization process, which consist of the outward growth of lamellar stacks.[33] The upward deviation at the end of the plots is mainly attributed to the secondary crystallization, which is caused by impingement and nonlinear growth patterns of spherulites in the later stage of the crystallization process.[34] The values of k and n can be calculated from the intercept and slope of the straight lines and are listed in Table 3. According to Table 3, the n values of PBT and PBT/TDP blends range from 2.24-2.84, indicating an athermal nucleation process followed by a hybrid crystal structure of planar lamellae and three-dimensional spherulitic growth.[33-35] And the values of n are non-integer in all cases, which may be a result of the mixed growth or surface nucleation of crystals [36, 37] and the crystalline branching or two-stage crystal growth during the crystallization process.[38] It is unscientific to compare the overall crystallization rate directly from the k values, because the unit of k is min^{-n} and n is a variable at different T_c in present work. Another important parameter is the half-time of crystallization ($t_{1/2}$), which is defined as the time at which the extent of crystallization is 50 %. It can be calculated from equation (7) which is derived from the Avrami equation and the values of $t_{1/2}$ are listed in Table 3. Generally, the reciprocal of $t_{1/2}$ is taken as a parameter of the crystallization rate of polymer,[14, 39, 40] the relation of $1/t_{1/2}$ and T_c is shown in Fig. 7. The values of $1/t_{1/2}$ decrease with the increasing weight fraction of TDP at the same T_c (198-206°C). when T_c =198°C, pure PBT shows a $1/t_{1/2}$ of 1.51 min^{-1}, while with the addition of 6 wt% TDP and $1/t_{1/2}$ decreases to 0.577 min^{-1}. The overall isothermal crystallization rates of PBT in PBT/TDP blends are obviously slower than that of pure PBT at the same crystallization temperature, indicating that crystallization of PBT is suppressed by the hydrogen-bonding interaction between the PBT and TDP. In addition, the values of $1/t_{1/2}$ gradually decreases with increasing T_c for pure and blended PBT, which should arise from the low supercooling at higher T_c.[40] In short, the blending with TDP inhibits the isothermal melt crystallization process of PBT in the blends.

$$t_{1/2} = (\frac{ln2}{k})^{1/n} \quad (7)$$

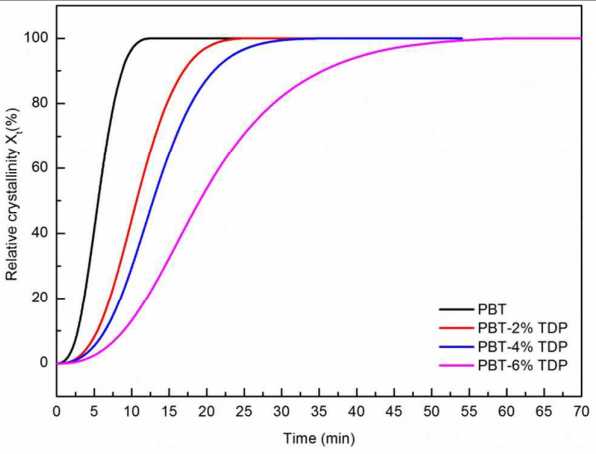

Fig. 5 Relative crystallinity of pure PBT and PBT/TDP blends as a function of time isothermally crystallized at 206 °C.

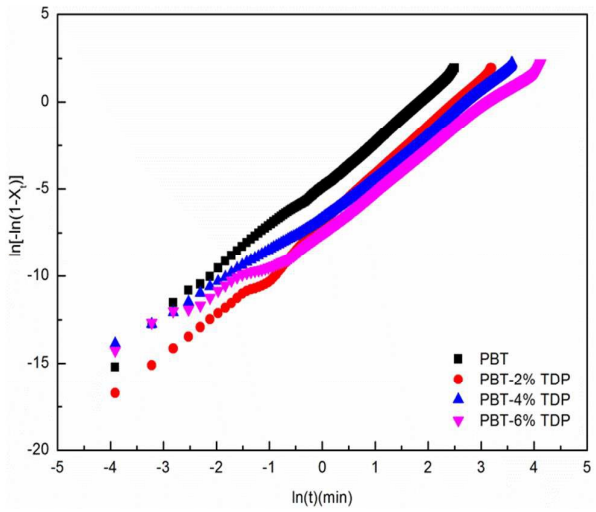

Fig. 6 Avrami analysis of pure PBT and PBT/TDP blends isothermally crystallized at 206 °C.

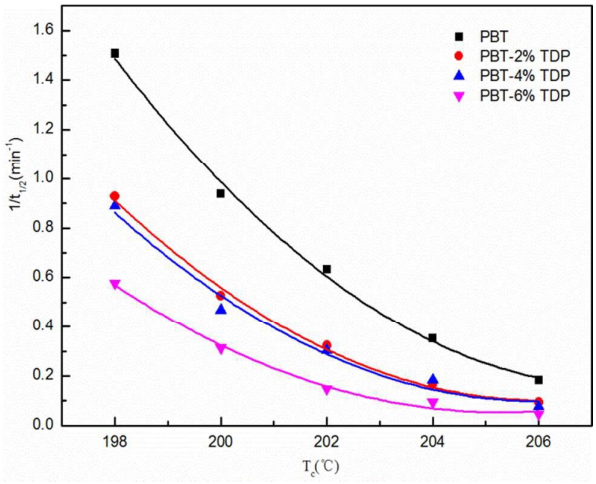

Fig. 7 Plots of $1/t_{1/2}$ versus T_c for pure PBT and PBT/TDP blends.

3.5 Wide-angle X-ray measurements

Fig. 8 shows X-ray diffractograms for PBT and PBT/TDP blends. The main peaks of PBT locate at around 15.9°, 17.2°, 20.4°, 23.2° and 24.8° correspond to the planes of $(01\bar{1})$, (010), $(10\bar{2})$, (100) and $(11\bar{1})$, respectively. The characteristic peaks of PBT/TDP blends are similar to those of neat PBT. There are no new characteristic peaks appearing in the X-ray patterns of the blends, indicating that the inclusion of TDP has little effect on the crystal structure of PBT， and TDP may exist in the amorphous region of PBT. Generally, XRD spectrum of samples with small crystallite size have wide, low intensity diffraction peak profiles and samples with large crystallite size have sharp, high intensity peak profiles.[11] It is clearly seen from Fig. 8 that the intensity of diffraction peaks weaken and the peak shapes become flat with increasing content of TDP, meaning that the crystallinity and the crystallite size of PBT reduce with the addition of TDP.

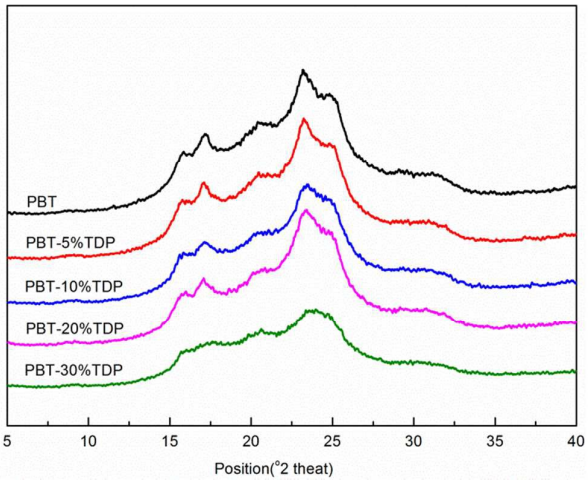

Fig. 8 WAXD curves for the PBT and PBT/TDP blends.

Table 3 Crystallization kinetic parameters of pure PBT and PBT/TDP blends at different temperatures

PBT/TDP (wt/wt %)	T_c(°C)	n	k (min^{-n})	$t_{1/2}$ (min)	$1/t_{1/2}$ (min^{-1})
100/0	198	2.65	20.6×10^{-1}	0.663	1.51
	200	2.62	5.85×10^{-1}	1.07	0.937
	202	2.47	2.25×10^{-1}	1.58	0.634
	204	2.62	4.49×10^{-2}	2.84	0.352
	206	2.60	8.21×10^{-3}	5.50	0.182
98/2	198	2.40	5.77×10^{-1}	1.08	0.927
	200	2.68	1.23×10^{-1}	1.90	0.526
	202	2.42	4.49×10^{-2}	3.10	0.323
	204	2.57	6.95×10^{-3}	6.00	0.167
	206	2.74	1.01×10^{-3}	10.8	0.0926
96/4	198	2.63	5.10×10^{-1}	1.12	0.890
	200	2.86	7.94×10^{-2}	2.14	0.468
	202	2.61	3.07×10^{-2}	3.29	0.304
	204	2.55	9.15×10^{-3}	5.46	0.183
	206	2.42	1.37×10^{-3}	13.1	0.0763
94/6	198	2.43	1.83×10^{-1}	1.73	0.577
	200	2.48	3.91×10^{-2}	3.18	0.314
	202	2.50	5.78×10^{-3}	6.77	0.148
	204	2.29	3.11×10^{-3}	10.6	0.0943
	206	2.24	7.67×10^{-4}	20.8	0.048

3.6 Polarized optical microscopy

The crystallization morphology of pure PBT and PBT/TDP blends isothermally crystallized at 202°C for 10 min is shown in Fig. 9. It can be seen that the size of spherulites in PBT/TDP blends is smaller than that of pure PBT, which is in accordance with XRD analysis. The observed result of smaller spherulites size can be related to the cross-linking structure which formed in PBT/TDP blends because of the hydrogen-bonding interaction as shown in Fig. 10. And this possible cross- linking structure actually belongs to a type of physical cross-linking

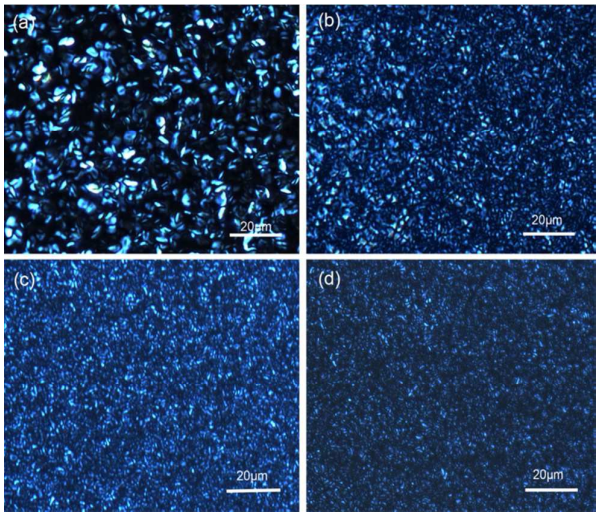

Fig.9 Polarized optical micrographs of PBT/TDP blends with different content of TDP: (a) 0 wt%; (b) 2 wt%; (c) 4 wt%; (d) 6 wt% isothermally crystallized at 202°C for 10min.

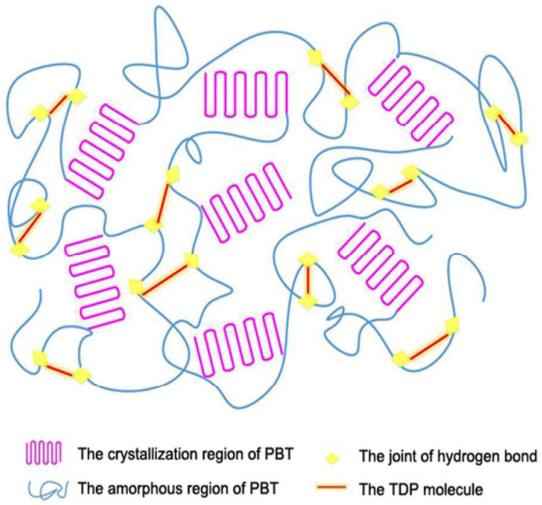

Fig. 10 The Schematic representation of the PBT-TDP inter-associated existence in the mixtures.

and probably hinders the movement of molecular chain and the growth of crystal and results in lower the crystallization rate. In addition, it can be observed that the more the TDP content is, the more blurry the blend crystal is. It may be because of more defects formation resulted from more hydrogen-bonding with increasing TDP content.

3.7 Elongation-at-break

The elongation-at-break (%) of PBT/TDP blends is showed in Fig. 11. An obvious dependence of the elongation-at-break of PBT on TDP content is observed and this dependence is embodied in the increasing elongation-at-break of blends with the increase of TDP content. The pure PBT shows an elongation-at-break of 449.7%, and with addition of 30 wt% TDP, the value of elongation-at-break reaches up to 736.2%, indicating the enhancement of ductility of the blend system.

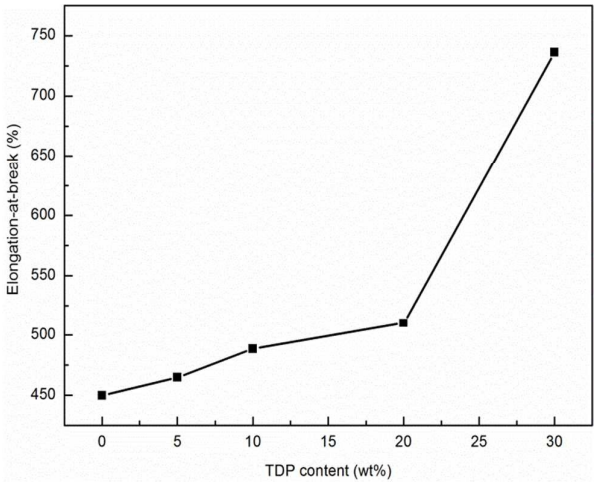

Fig. 11 Variations of elongation-at-break (%) of PBT/TDP blends.

4 Conclusions

Quantum-chemical calculation and FTIR analysis verified that intermolecular hydrogen-bonding formed between PBT and TDP. TDP could be regarded as an effective crystal mediator and significantly suppressed the crystallization properties of PBT. When TDP content reached to 30wt%, the crystallization temperature and crystallinity of PBT reduced 33°C and 17.52%, respectively. The elongation-at-break of PBT increases from 449.7% to 736.2%. For the overall isothermal crystallization process, the crystallization kinetics and spherulites morphology of PBT were obviously influenced by TDP content. The PBT/TDP blends had slower crystallization rate than pure PBT. The crystallite size of PBT decreased with the increasing of TDP content while the crystal structure of PBT did not change with the addition of TDP.

Acknowledgements

This work was gratefully supported by National Natural Science Foundation of China (Nos. 21264012 and 51403210).

References

1 J.-W. Huang, Y.-L. Wen, C.-C. Kang, M.-Y. Yeh and S.-B. Wen, *Journal of Applied Polymer Science*, 2008, **109**, 3070-3079.
2 T.-K. Kang, Y. Kim, W.-K. Lee, H.-D. Park, W.-J. Cho and C.-S. Ha, *Journal of Applied Polymer Science*, 1999, **72**, 989-997.
3 N. Tomar and S. N. Maiti, *Journal of Applied Polymer Science*, 2009, **113**, 1657-1663.
4 E. Gubbels, L. Jasinska-Walc, D. Hermida-Merino, M. R. Hansen, B. Noordover, A. Spoelstra, H. Goossens and C. Koning, *Polymer*, 2014, **55**, 3801-3810.
5 A. Ramani and A. E. Dahoe, *Polymer Degradation and Stability*, 2014, **104**, 71-86.
6 H. Bai, Y. Zhang, Y. Zhang, X. Zhang and W. Zhou, *Journal of Applied Polymer Science*, 2006, **101**, 54-62.
7 J.-W. Huang, Y.-L. Wen, C.-C. Kang, M.-Y. Yeh and S.-B. Wen, *Journal of Applied Polymer Science*, 2008, **107**, 583-592.
8 W. S. Chow, *Journal of Applied Polymer Science*, 2008, **110**, 1642-1648.
9 H. Fang and F. Wu, *Journal of Applied Polymer Science*, 2014, **131**, 40849-40859.
10 J. Bian, H. L. Lin, F. X. He, L. Wang, X. W. Wei, I.-T. Chang and E. Sancaktar, *European Polymer Journal*, 2013, **49**, 1406-1423.
11 G. S. Deshmukh, D. R. Peshwe, S. U. Pathak and J. D. Ekhe, *Thermochimica Acta*, 2014, **581**, 41-53.
12 G. S. Deshmukh, D. R. Peshwe, S. U. Pathak and J. D. Ekhe, *Thermochimica Acta*, 2015, **606**, 66-76.
13 B. Kulshreshtha, A. K. Ghosh and A. Misra, *Polymer*, 2003, **44**, 4723-4734.
14 F.-l. Luo, F.-h. Luo, Q. Xing, X.-q. Zhang, H.-q. Jiao, M. Yao, C.-t. Luo and D.-j. Wang, *Chinese Journal of Polymer Science*, 2013, **31**, 1685-1696.
15 J. Li, Y. He and Y. Inoue, *Journal of Polymer Science Part B: Polymer Physics*, 2001, **39**, 2108-2117.
16 Y. He, N. Asakawa and Y. Inoue, *Journal of Polymer Science Part B: Polymer Physics*, 2000, **38**, 2891-2900.
17 Y. He, N. Asakawa, J. Li and Y. Inoue, *Journal of Applied Polymer Science*, 2001, **82**, 640-649.
18 Y. Zhao and D. Truhlar, *Theor Chem Account*, 2008, **120**, 215-241.
19 J. A. Plumley and J. J. Dannenberg, *Journal of Computational Chemistry*, 2011, **32**, 1519-1527.
20 M. Walker, A. J. A. Harvey, A. Sen and C. E. H. Dessent, *The Journal of Physical Chemistry A*, 2013, **117**, 12590-12600.
21 M. J. Frisch, G. W. Trucks, H. B. Schlegel, G. E. Scuseria, M. A. Robb, J. R. Cheeseman, G. Scalmani, V. Barone, B. Mennucci, G. A. Petersson, H. Nakatsuji, M. Caricato, X. Li, H. P. Hratchian, A. F. Izmaylov, J. Bloino, G. Zheng, J. L. Sonnenberg, M. Hada, M. Ehara, K. Toyota, R. Fukuda, J. Hasegawa, M. Ishida, T. Nakajima, Y. Honda, O. Kitao, H. Nakai, T. Vreven, J. A. Montgomery, Jr., J. E. Peralta, F. Ogliaro, M. Bearpark, J. J. Heyd, E. Brothers, K. N. Kudin, V. N. Staroverov, R. Kobayashi, J. Normand, K. Raghavachari, A. Rendell, J. C. Burant, S. S. Iyengar, J. Tomasi, M. Cossi, N. Rega, J. M. Millam, M. Klene, J. E. Knox, J. B. Cross, V. Bakken, C. Adamo, J. Jaramillo, R. Gomperts, R. E. Stratmann, O. Yazyev, A. J. Austin, R. Cammi, C. Pomelli, J. W. Ochterski, R. L. Martin, K. Morokuma, V. G. Zakrzewski, G. A. Voth, P. Salvador, J. J. Dannenberg, S. Dapprich, A. D. Daniels, O. Farkas, J. B. Foresman, J. V. Ortiz, J. Cioslowski, D. J. Fox, Gaussian 09, Gaussian, Inc., WallingfordCT, 2009.
22 S. S. Batsanov, *Inorganic Materials*, 2001, **37**, 871-885.
23 Y. He, N. Asakawa and Y. Inoue, *Journal of Polymer Science Part B: Polymer Physics*, 2000, **38**, 1848-1859.
24 B. Hexig, Y. He, N. Asakawa and Y. Inoue, *Journal of Polymer Science Part B: Polymer Physics*, 2004, **42**, 2971-2982.
25 S.-F. Wen, *Fourier transform infrared spectroscopy*, Chemical Industry Press, Bei Jing, 2010.
26 H. Yan, J. Xu, K. Mai and H. Zeng, *Polymer*, 1999, **40**, 4865-4875.
27 H. Bai, Y. Zhang, Y. Zhang, X. Zhang and W. Zhou, *Journal of Applied Polymer Science*, 2006, **101**, 1295-1308.
28 K.-H. Illers, *Colloid and Polymer Science*, 1980, **258**, 117-124.
29 M. C. Righetti and A. Munari, *Macromolecular Chemistry and Physics*, 1997, **198**, 363-378.
30 S. S. Iyengar, H. B. Schlegel, J. M. Millam, G. A. Voth, G. E. Scuseria and M. J. Frisch, *The Journal of Chemical Physics*, 2001, **115**, 10291-10302.
31 H. B. Schlegel, J. M. Millam, S. S. Iyengar, G. A. Voth, A. D. Daniels, G. E. Scuseria and M. J. Frisch, *The Journal of Chemical Physics*, 2001, **114**, 9758-9763.
32 H. B. Schlegel, S. S. Iyengar, X. Li, J. M. Millam, G. A. Voth, G. E. Scuseria and M. J. Frisch, *The Journal of Chemical Physics*, 2002, **117**, 8694-8704.
33 P.-D. Hong, W.-T. Chung and C.-F. Hsu, *Polymer*, 2002, **43**, 3335 - 3343.
34 J. Dou and Z. Liu, *Polymer International*, 2013, **62**, 1698-1710.
35 X. Xiao, Z. Zeng, W. Xue, Q. Kong and W. Zhu, *Polymer Engineering & Science*, 2013, **53**, 482-490.

36 S.-W. Kuo, S.-C. Chan and F.-C. Chang, *Journal of Polymer Science Part B: Polymer Physics*, 2004, **42**, 117-128.
37 S.-W. Kuo, S.-C. Chan and F.-C. Chang, *Macromolecules*, 2003, **36**, 6653-6661.
38 R. G. Alamo and L. Mandelkern, *Macromolecules*, 1991, **24**, 6480-6493.
39 J. W. Huang, Y. L. Wen, C. C. Kang, M. Y. Yeh and S. B. Wen, *Journal of Applied Polymer Science*, 2008, **109**, 3070-3079.
40 Y. Zhao and Z. Qiu, *RSC Adv.*, 2015, **5**, 49216-49223.

Graphical Abstract

The intermolecular hydrogen-bonding formed between PBT and TDP can efficiently mediate the crystallization behavior of PBT.